HHS Public Access

Author manuscript

Adv Funct Mater. Author manuscript; available in PMC 2022 May 06.

Published in final edited form as:

Adv Funct Mater. 2020 September 03; 30(36): . doi:10.1002/adfm.202000577.

Magnetothermal Multiplexing for Selective Remote Control of Cell Signaling

Junsang Moon[†,‡,§], **Michael G. Christiansen**[‖], **Siyuan Rao**[‡,§], **Colin Marcus**[†,¶], **David C Bono**[†], **Dekel Rosenfeld**[‡,§], **Danijela Gregurec**[‡,§], **Georgios Varnavides**[†,‡,§], **Po-Han Chiang**[‡,§,#], **Seongjun Park**[‡,§,††,‡‡], **Polina Anikeeva**[†,‡,§,§§]

[†]Department of Materials Science and Engineering, Massachusetts Institute of Technology, Cambridge, MA, USA

[‡]Research Laboratory of Electronics, Massachusetts Institute of Technology, Cambridge, MA, USA

[§]McGovern Institute for Brain Research, Massachusetts Institute of Technology, Cambridge, MA, USA

[‖]Department of Health Sciences and Technology, Swiss Federal Institute of Technology, 8093 Zürich, Switzerland

[¶]Computer Science and Artificial Intelligence Lab, Massachusetts Institute of Technology, Cambridge, MA, USA

[#]Institute of Biomedical Engineering, National Chiao Tung University, 1001 University Road, Hsinchu, Taiwan 30010

[††]Department of Electrical Engineering and Computer Science, Massachusetts Institute of Technology, Cambridge, MA, USA

[‡‡]Department of Bio and Brain Engineering, Korea Advanced Institute of Science and Technology, Daejeon 34141, Republic of Korea

[§§]Department of Brain and Cognitive Sciences, Massachusetts Institute of Technology, Cambridge, MA, USA

Abstract

Magnetic nanoparticles have garnered sustained research interest for their promise in biomedical applications including diagnostic imaging, triggered drug release, cancer hyperthermia, and neural stimulation. Many of these applications make use of heat dissipation by ferrite nanoparticles under alternating magnetic fields, with these fields acting as an externally administered stimulus that is either present or absent, toggling heat dissipation on and off. Here, we motivate and demonstrate an extension of this concept, magnetothermal multiplexing, in which exposure to alternating magnetic fields of differing amplitude and frequency can result in selective and independent heating of magnetic nanoparticle ensembles. The differing magnetic coercivity

Supporting Information

Supporting Information is available from the Wiley Online Library or from the author.

of these particles, empirically characterized by a custom high amplitude alternating current magnetometer, informs the systematic selection of a multiplexed material system. This work culminates in a demonstration of magnetothermal multiplexing for selective remote control of cellular signaling *in vitro*.

Graphical Abstract

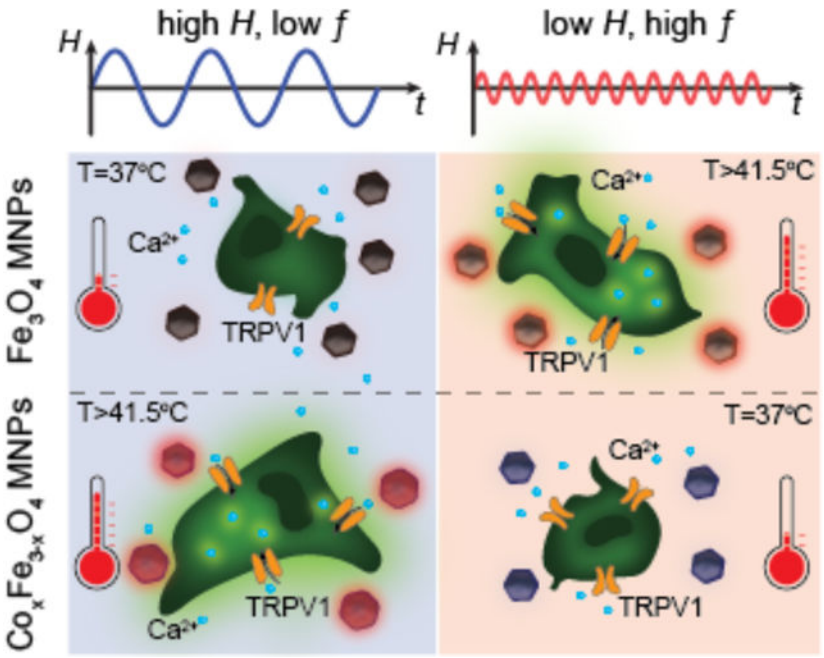

Keywords

magnetic nanoparticle; multiplexed magnetothermal control; AC magnetometer; selective nanoparticle heating; cellular signaling control

1. Introduction

Heat dissipation by magnetic nanoparticles (MNPs), while historically focused on tissue ablation, has increasingly served to couple or actuate biological responses with noninvasive alternating magnetic fields (AMFs).[1–3] These emerging applications typically employ a predefined AMF and a single type of MNP. Consequently, efforts in advancing MNP synthesis chemistry have focused on maximizing heat dissipation under a single AMF condition. In contrast, the ability to selectively heat MNPs with differing coercivities using distinct AMF conditions, “magnetothermal multiplexing,” can offer independent control over multiple processes. We previously applied a dynamic magnetization model to conceptually demonstrate this possibility.[4] However, practical realization of magnetothermally multiplexed control additionally requires a robust process for optimization and experimental validation of selective response in model systems.

Here, we present a systematic approach for developing materials for magnetothermal multiplexing. Our methodology is enabled by the development of a model that predicts dynamic magnetization response at applied AMFs, a high amplitude magnetometer, and a framework for quantitatively comparing multiplexing performance. Using materials and AMF conditions identified for multiplexing, we demonstrate selective heating of two neighboring ferrofluids and independent actuation of calcium ion influx in two heat-sensitized cell populations.

When MNPs are exposed to AMFs, they dissipate heat arising from thermodynamic irreversibility in the response of their magnetization. This irreversibility can be graphically represented by hysteresis loops, which enclose an area corresponding to the heat dissipated per magnetization cycle. While all models for heat dissipation by MNPs can be understood as methods for predicting hysteresis loops, the “dynamic hysteresis” model does this by describing magnetization response as a kinetic process determined by an energy landscape consisting of the effective anisotropy energy and the configurational energy of the MNP moment in the applied AMF (Supporting Information).[4,5] The relevant energy contributions depend on the MNP materials properties (effective magnetic anisotropy K_{eff}, saturation magnetization M_s, volume V), temperature T, and the applied AMF conditions (field amplitude H and frequency f). Major hysteresis loops are observed when AMF amplitude is sufficient to overcome the anisotropy barrier to magnetization reversal, whereas lower AMF amplitudes yield only minor loops with comparatively smaller areas.[4,5] If effective magnetic anisotropy K_{eff} is increased while magnetization remains constant, the major hysteresis loops are expanded, and an increase in AMF amplitude is required to access them.

Provided that the AMF amplitude-frequency product is constrained to mitigate off-target heat dissipation, [6] MNPs heat optimally in AMFs with the minimum amplitude required to access their major hysteresis loops and the highest permissible frequency. For MNPs composed of magnetic ferrites ($A_xFe_{3-x}O_4$, A = Co, Mn, Ni, $x \leq 1$) K_{eff} can be manipulated by introducing transition metals into iron oxide.[7] In particular, Co is known to induce the largest change in the first order cubic anisotropy constant (2.6×10^5 Jm^{-3} for stoichiometric $CoFe_2O_4$) compared to other transition metals.[8] Cobalt substitution into Fe_3O_4 breaks d-orbital degeneracy, leading to stronger spin-orbit coupling, increased magnetic anisotropy, and expanded hysteresis loops (Figure 1a, b).[9–11] Engineering magnetic anisotropy produces MNPs with sufficiently distinct optimal AMF conditions to enable selective heating. Based on this reasoning, we developed a materials-based system consisting of MNP ensembles with low- and high-K_{eff} (Figure 1a, b). High-K_{eff} MNPs dissipate heat most efficiently in response to AMFs with high amplitude and low frequency ($H_{high}\, f_{low}$, Figure 1c), whereas low-K_{eff} MNPs dissipate heat most efficiently in response to AMFs with low amplitude and high frequency ($H_{low}\, f_{high}$, Figure 1d).

We then experimentally demonstrated multiplexed magnetothermal control over two neighboring ferrofluids and numerically investigated the effects of proximity on independent actuation. Finally, we applied magnetothermal multiplexing to selectively modulate signaling in two populations of human embryonic kidney cells (HEK293FT) transfected to express a transient receptor potential vanilloid family member 1 (TRPV1). This cation

channel is sensitive to heat and capsaicin, transporting divalent cations such as Ca^{2+} across the membrane at temperatures exceeding 41.5±1.1 °C.[12] Thermal activation of TRPV1 can be inferred from Ca^{2+} influx observed via increased fluorescence of a coexpressed calcium indicator GCaMP6s.[3,13] Surrounding the heat-sensitized cells with solutions of either low-K_{eff} or high-K_{eff} MNPs enabled observation of a selective response to the AMF conditions paired with the surrounding ferrofluid (Figure 1c and d).

2. Results and Discussion

2.1. Preparation of candidate nanoparticles for multiplexing

To identify two MNP ensembles suitable for magnetothermal multiplexing, we synthesized an array of magnetite (Fe_3O_4) and cobalt doped ferrite ($Co_xFe_{3-x}O_4$, $0<x<1$) nanoparticles with varied dimensions and Co content (Figure 2a–h). X-ray powder diffraction (XRPD) confirmed the inverse spinel crystal structure of the magnetite and cobalt ferrite MNPs (Figure 2i). This finding was additionally consistent with a comparison of the effective MNP magnetic moments to the expected magnetic moments assuming bulk material M_s (Figure S1).[8,14] An increase in the coercive field (H_c) for cobalt ferrite MNPs was observed for samples in which physical rotation of MNPs was prevented (Figure 2j). Cobalt concentration in the MNPs was controlled stoichometrically during synthesis and corroborated by inductively coupled plasma atomic emission spectroscopy (ICP-AES) (Figure 2k). To ensure colloidal stability in aqueous solutions, MNPs were coated with a biodegradable amphiphilic polymer poly(maleic anhydride-alt-1-octadecene) (PMAO) covalently linked to poly(ethylene glycol) methyl ether (mPEG).[15]

2.2. Characterization of dynamic magnetization

To characterize the heating of MNPs under various AMF conditions, we directly captured dynamic hysteresis loops of samples with a custom high-amplitude alternating current (AC) magnetometer. While previous studies have made use of AC magnetometers, [16–20] our instrument accessed a significantly expanded range of AMF amplitudes and frequencies (≤ 214mT at 23.3kHz, ≤ 153mT at 75kHz, ≤ 84.8mT at 174.3kHz, ≤ 26.2mT at 488.5kHz and ≤ 19.5mT at 565.4kHz) facilitating rapid identification of MNP materials and paired driving conditions for multiplexing.

The electromagnet in our custom AC magnetometer generated a uniform AMF within the gap of a soft ferromagnetic core (Figure 3a and Figure S2a,b). For small working volumes, [21] such a design lowers the power required to reach relevant AMF amplitudes compared to previously reported air core designs. [16,17,20] Instead of using a pair of coaxial solenoids as sense and compensation coils as is typical, [16] our design employed a symmetric set of side-by-side spirals on a printed circuit board precisely positioned within the electromagnet gap via a printed holder (Figure 3a and b). The voltage produced by the field in the compensation coil partially canceled the field induced in the sense coil, isolating the signal arising from the time-varying magnetization of a MNP sample (Figure 3b). The circuit board containing the coils amplified the signal to facilitate detection.

AC magnetometry revealed the dynamic magnetization behavior of a ferrofluid, which differed from the slow magnetization response of the MNPs measured by VSM. The time allowed for physical rotation during VSM measurements ensured almost no hysteresis for all particle ensembles (Figure 3c, d and Figure S3). In contrast, the AC magnetometer revealed the dynamic response and hysteretic behavior of MNP ensembles at precisely the conditions of interest (Figure 3c, d). To validate the hysteresis loops collected by our AC magnetometer, we compared heating efficiencies (specific loss powers (SLPs) in W/g_{Metal}) of MNP ensembles calculated from the hysteresis loop areas to values determined calorimetrically via direct measurement of temperature change in thermally insulated ferrofluids exposed to identical AMF conditions (Figure 3e, g). SLPs measured by both methods were in quantitative agreement.

Increasing Fe_3O_4 MNP size (16.3±0.7, 20.5±1.3, 25.2±1.4, and 31.2±2.3 nm) and K_{eff} by the addition of Co ($Co_xFe_{3-x}O_4$, x = 0.01, 0.03, 0.14, and 0.24) resulted in higher coercive fields (H_c) and larger hysteresis loop areas (Figure 3e,g,i,k). These observations are consistent with the predictions of the dynamic hysteresis model (Figure 3f,h,j,l and Figure S3a–h.).[4,5] Increasing K_{eff} via cobalt doping yields a more marked expansion of hysteresis loop area than increasing particle size. This is expected because, unlike a volume increase, cobalt doping increases the anisotropy energy without increasing the MNP magnetic moments.

Agreement between the observed and predicted hysteretic behaviors, both in the changes of coercivities and trends in SLP versus AMF amplitude, suggests that our model offers a viable foundation for identifying AMF conditions maximizing SLPs of these materials. Accordingly, we selected the MNPs for magnetothermal multiplexing with the most disparate coercivities from our synthesized particle set in Figure 2a–h. MNPs of Fe_3O_4 with diameters of 16.3±0.7 nm were chosen as the low-coercivity MNP_1 due to their low volume and low-K_{eff} (Figure 3e). MNPs of $Co_{0.24}Fe_{2.76}O_4$ with diameters of 18.6±1.1 nm were selected as the high-coercivity MNP_2 due to their high Co content, resulting in the highest K_{eff} and widest dynamic hysteresis loops (Figure 3g).

2.3. Determination of suitable AMF conditions for selective heating

Hysteresis loops of MNPs driven by AMFs do not vary markedly with frequency within the kHz range, [16,18,19,22] an observation substantiated with both AC magnetometry and direct calorimetry (Figure 3e, g). Leveraging this fact, we used AC magnetometry data to extrapolate SLPs of MNP_1 (16.3 nm Fe_3O_4) and MNP_2 (18.6 nm $Co_{0.24}Fe_{2.76}O_4$) to a range of AMF conditions accessible in our *in vitro* imaging apparatus (AMF amplitude $H \leq 70$ kA/m) by multiplying hysteresis loop areas by the frequencies. All considered AMF conditions fell below the therapeutically acceptable amplitude-frequency product ($H \cdot f < 5\times10^9$ kAm^{-1} s^{-1}).[6] To facilitate quantitative comparison of multiplexing performance, a multiplexing factor (MF) was defined as a function of ratios of expected SLPs such that it was maximized for AMF conditions producing selective heating in both materials (Supporting Information and Figure S4, 5). Frequency pairs for MNP_1 and MNP_2 were selected first to 522 kHz and 50 kHz, based on preliminary scanning of MF calculated from AC magnetometer measurements for MNPs. (Supporting Information and Figure S4). Figure

4a illustrates the variation of the MF for AMFs with frequencies set to f_1 = 522 kHz and f_2 = 50 kHz, and amplitudes varying between 0–70 kA/m (Figure S5). Using this plot, we selected AMF conditions of H_1 = 10kA/m, f_1 = 522 kHz (AMF_1) and H_2 = 70 kA/m, f_2 = 50 kHz (AMF_2) to selectively drive heating of the MNP_1 and MNP_2 ensembles.

We then verified that the MNP_1 (20.2 mg_{Metal}/ml in water) and MNP_2 (10.5 mg_{Metal}/ml in water) could selectively respond to AMF_1 and AMF_2 by exposing their droplets (10 μl each) to either of the selected AMF conditions for 20s. The temperatures of the solutions were recorded in real time using an infrared camera. As shown in Figure 4b, c, Figure S6 and Supplementary Video S1, each MNP droplet heats significantly ($\Delta T_{MNP1\text{-}AMF1} \approx 19.6$ °C, $\Delta T_{MNP2\text{-}AMF2} \approx 18.6$ °C) only when exposed to its paired AMF.

To assess future utility of magnetothermal multiplexing as a means to control independent biological processes, we explored the extent of the cross-talk between the neighboring ferrofluid droplets. While future advances may enable applications of individual MNPs targeted to distinct cells within mixed ensembles, these studies rely on expanded understanding of the heat transport at the nanoscale.[23–26] To date, however, concentrated ferrofluids have shown most promise for heat-mediated cellular modulation *in vivo*[3,27,28], and consequently we investigate their utility for independently controlling distinct organ regions. Because heat can be transferred through tissue or media to neighboring regions, the distance between two droplets is an important consideration for preventing crosstalk. Direct measurement of 3D temperature profiles resulting from embedded heat-generating ferrofluid droplets is challenging, particularly in the context of a living organism. Instead, we simulated this multiplexed magnetothermal modulation in the model of a mouse brain using finite element analysis to solve Pennes' bioheat equation with a combination of our empirical data and parameters from literature[3,29] (Supplementary Video S2 and Figure S7). Prior work has shown that 1 μL ferrofluid injection into a deep brain structure within a mouse brain is sufficient to mediate triggering of heat-sensitized neurons in the presence of an AMF without causing adverse effects.[3] Therefore, we simulated two 1 μL ferrofluid droplets. When the surfaces of 1 μL droplets are separated by 2 mm, heat generated from one source did not substantially affect the other droplet's thermal profile (Figure S7a–c). Given the temperature thresholds of heat-sensitive ion channels further reduction in the separation between the ferrofluid droplets is possible. This result implies that the characterized magnetothermal multiplexing system can be applied to selectively modulate organ regions separated by 2 mm (Figure S7 d).

2.4. Multiplexed magnetothermal control of cell signaling

To evaluate the potential of magnetothermal multiplexing as a means to independently control cell signaling, we first corroborated the biocompatibility of our ferrofluids in cultures of HEK293FT cells (Figure S8). We then applied multiplexed magnetothermal control to HEK293FT cells co-transfected with heat-sensitive cation channel TRPV1 and a calcium indicator GCaMP6s (Figure 5a–c). These cells, prepared on glass coverslips coated with Matrigel®, were submerged within dilute ferrofluids of MNP_1 (6.6 mg_{Metal}/ml in Tyrode's solution) or MNP_2 (3.8 mg_{Metal}/ml in Tyrode's solution) and exposed to the AMF_1 and AMF_2. To eliminate the possible influence of variability in response between different

cell populations, each sample was first exposed to its unpaired AMF condition predicted to yield negligible heating of the ferrofluid, followed by exposure to the paired AMF known to produce efficient heat dissipation in the given MNP solution. GCaMP6s fluorescence dynamics within cell populations (n=100 cells from 8 coverslips per ferrofluid) were recorded over the entire experiment duration using an inverted fluorescence microscope.

Thermal triggering of TRPV1 was expected to induce intracellular Ca^{2+} influx, [3,30] which was observed via a change in GCaMP6s fluorescence (ΔF) for each cell within a field of view normalized to its initial background fluorescence (F_0). Consistent with the temperature changes in the surrounding ferrofluids, a strong response was observed only when the AMF conditions were optimized for the given MNP (Figure 5d–g). When exposed to AMF_1, MNP_1 solutions increased in temperature by ~ 6.4 °C, reaching T=43.6 °C in 20 s, triggering Ca^{2+} influx through TRPV1 and significantly increasing GCaMP6s fluorescence (Figure 5d and Supplementary Video S3). In contrast, exposure of MNP_1 ferrofluid to AMF_2 increased the temperature by only ~1.5 °C, which was insufficient to trigger TRPV1 (Figure 5e and Supplementary Video S4). Conversely, MNP_2 ferrofluid exhibited negligible heating of ~1.2 °C upon exposure to AMF_1, insufficient to excite Ca^{2+} influx within the submerged cell populations (Figure 5f and Supplementary Video S5). Exposure to AMF_2 evoked a temperature increase of 6.6 °C (to T=43.8 °C in 20 s), which triggered TRPV1 opening, Ca^{2+} influx, and an increase in GCaMP6s fluorescence in 67% of analyzed cells (Figure 5g and Supplementary Video S6).

While our ability to simultaneously expose two cell populations to both AMFs was limited by our experimental apparatus, our in situ measurements (Figure 4) and modeling results (Figure S7) suggest that the selective response of the cells surrounded by the distinct ferrofluids to their paired AMF conditions (Figure 5) is a viable means of multiplexed magnetothermal control of organ regions.

3. Conclusions

This work has demonstrated a nanomaterials-based approach to selectively heat MNP ensembles with distinct magnetic properties. Our strategy relied on manipulating coercivity by controlling particle size and cobalt incorporation into magnetite. A methodology to determine suitable AMF conditions was implemented, relying on a custom-designed high amplitude AC magnetometer that revealed dynamic magnetization behavior and provided a basis for empirical extrapolation. The utility of the selected materials was shown *in vitro* as a means to independently evoke intracellular Ca^{2+} influx into heat-sensitized cell populations surrounded by distinct ferrofluids with paired AMF conditions. While we chose control of cell signaling as a testbed, the approach and underlying principles are generalizable to numerous applications employing MNP ensembles as heat sources. This includes sequential release of pharmacological compounds in multiple target regions or stimulation of multiple sub-structures of organs including the nervous system.[31,32] Various alternative synthetic routes to MNPs with differing coercivities are available. For instance, a recent study on magnetosomes that are ultimately converted by stem cells to smaller magnetite particles may suggest a means to selectively modulate cells based on their metabolic processes.[33] For applications in which it is challenging to superimpose a magnetostatic field to achieve

spatial selectivity of thermal modulation,[34] such as in moving objects or in freely behaving subjects, magnetothermal multiplexing may offer an attractive alternative for selective heating of MNP ensembles.

Experimental Section

Materials:

Solvents were purchased from Sigma-Aldrich - Oleic acid (90%), 1-octadecene (90%) and benzyl ether (98%). Sodium oleate (95%, TCI America), iron chloride hexahydrate (99%, Acros), poly(maleic anhydride-alt-1-octadecene, Sigma-Aldrich) (Mn=30,000~50,000) and poly(ethylene glycol) methyl ether (Mn=5,000) were purchased from the stated vendors. All chemicals were used as received without additional purification.

Preparation of metal-oleate complex:

15-x mmol of $FeCl_3 \cdot 6H_2O$, x mmol of $CoCl_2 \cdot 6H_2O$ and 46-x mmol of sodium oleate were mixed with 100ml of hexane, 50ml of ethanol and 100ml of distilled water in a 250ml 3 neck round bottomed flask. The mixture was refluxed at 60°C for an hour under N_2. The metal-oleate complex dissolved in the hexane-rich top layer were collected in a separatory funnel and thoroughly washed 3 times with ddH_2O. The metal-oleate mixture was heated to 110 °C in a beaker overnight to remove hexane and other residual solvents.

Synthesis of nanoparticles:

Magnetic nanoparticles were prepared in a similar way as reported before. [35] In brief, 5mmol of iron oleate precursor was dissolved in a 250ml 3 neck round bottomed flask with 10ml of 1-octadecene and 5ml of benzyl ether. To control the size of the particles resulting from synthesis, oleic acid was added from 2.5mmol to 10mmol. The solution was degassed under vacuum for 30 to 60min at 90 °C, and then purged with N_2 gas. After purging, the temperature was increased up to 200 °C then it was set to heat up with 3.3°C/min rate, up to reflux temperature and held for 25min after reaching the temperature plateau associated with initial reflux. (Overall ~1hr after reaching 200 °C) Synthesized particles were washed by repeated dispersion in hexane and precipitation in ethanol, then spun down at 9,000 rpm (8694 rcf) for 15min. Washing steps were repeated at least 3 times, until the solvent looked transparent. The nanoparticle pellet was then collected and re-dispersed in chloroform. Particles in chloroform were stored at 4 °C.

Structural characterization:

Powder x-ray diffraction data were collected using Bruker-AXS Smart Apex charged-coupled device (CCD) detector with graphite monochromated Mo Kα radiation (λ = 0.71073 Å) for the structure of Fe_3O_4 and Co-doped Fe_3O_4. TEM images were collected by FEI Tecnai on an amorphous carbon TEM grid.

Phase transfer of nanoparticles:

Amphiphilic polymer, poly(ethylene glycol) methyl ether grafted poly(maleic anhydride-alt-1-octadecene) (mPEG-PMAO) was prepared by a similar protocol to previous studies.

[36] Magnetic nanoparticles (2~5mg) were dispersed in 1ml of mPEG-PMAO dissolved chloroform (concentration 10mg/ml). The mixture was sonicated for 15 minutes and then evaporated under vacuum. 1ml of 1x Tris-acetate-EDTA (TAE) buffer was added and sonicated for re-dispersion. Magnetic nanoparticles were spun down and washed 3 times with ddH_2O. For the *in vitro* experiment, MNPs were re-dispersed in Tyrode's solution in the final step.

Alternating current magnetometer measurements:

A custom designed AC magnetometer was built using 2 layer, 8mm thick printed circuit boards. Signals collected by the coil were also amplified by integrated circuit chips incorporated into the PCB. The sample holder, which contains a hollow sphere for ferrofluid injection was prepared by a 3D printer (Formlabs Form 2). After the cavity was filled with ferrofluid, it was sealed with a glue gun. The AC magnetometer was placed in the center of the gap of the electromagnet generating the AMF with the filled holder inside. The signal from a control sample (water) was subtracted from the signals measured from samples to isolate signal coming from dynamic magnetization of the MNPs.

Specific loss power measurements:

Phase transferred ferrofluid solutions were concentrated/diluted to ~2mg_{Metal}/ml. A custom-made series resonant circuit powered by 200W amplifier (1020L, Electronics & Innovation) receiving a sinusoidal signal from a function generator (Keysight 33210A) produced an alternating magnetic field. Field strength was adjusted by monitoring voltage induced in a pickup coil connected to oscilloscope (Keysight DSO-2004A). Temperature profiles were collected by fiber optic IR thermometer (Omega HHTFO-101), which is insensitive to alternating magnetic fields.

Dynamic magnetization calculations:

To investigate the dynamic magnetization response and hysteresis of single domain magnetic nanoparticles exposed to alternating magnetic fields, we conducted numerical calculation based on a dynamic magnetization model using Mathematica. [4,5] To simplify the model, magnetic anisotropy was approximated with an effective uniaxial anisotropy. Additionally, relaxation time τ_0 was not fixed to 10^{-9} s because relaxation time varies when exposed to external field. Details of the parameters can be found in Supporting Information.

Thermographic recording:

An infrared camera (FLIR ThermaCAM S60) was used to record selective magnetothermal heating of two ferrofluid droplets (10 μl of Fe_3O_4 and $Co_{0.24}Fe_{2.76}O_4$, 20.2 mg_{Metal}/ml and 10.5mg_{Metal}/ml in water each). The electromagnet generating the AMF was custom-built with a gapped toroidal core and wrapped with wires. Baseline temperature drift was adjusted by subtracting average temperature profile of background (entire field of view). (Figure S6a) Droplets were placed within the gap as seen in Figure S6b and Supplementary Video S1.

In vitro. Experiments:

HEK293FT cells were grown on 3mm cover slip coated with Matrigel using DMEM + 10% FBS medium. After 70% coverage of the cells was reached, they were transfected with TRPV1-p2A-mCherry and gCaMP6s using lipofectamine. During the experiment, coverslips with transfected cells were moved into a well placed in the center of the gap of the custom electromagnet generating the AMF and the well was filled with magnetic nanoparticles dispersed in Tyrode's solution. Dynamic fluorescence changes of gCaMP6s were observed with Olympus IX73 inverted microscope. Each coverslip immersed in MNP Tyrode's solution was stabilized to 37 °C before each stimulation, then exposed to AMF twice sequentially for 20s seconds, with the AMF expected to heat the MNPs inefficiently, and next with the AMF expected to heat the MNPs efficiently in the same FOV. Every cell was tracked individually to compare responses at each AMF condition. Temperature was recorded simultaneously in every trial using a fiber optic IR thermometer (Omega HHTFO-101). Each MNP ensemble was tested with 8 cell colonies. 100 cells were randomly selected by MATLAB code. F_0 for each cell was defined by the average fluorescence of the first 10s before applying an AMF.

Elemental analysis:

Nanoparticles were dissolved in 37% HCl then diluted with 2wt% Nitric acid solution to 1~100ppm range. Inductively Coupled Plasma-Optical Emission Spectrometer (Sistema ICP-OES Agilent 5100) was used to precisely quantify the metal content.

Biocompatibility test:

HEK293T cells were grown in 24-well plates in 10% Fetal bovine serum (FBS) + Dulbecco's modified eagle's medium (DMEM) up to 50% coverage. Cell medium was replaced on day1 and day 2 with 1ml MNP solution ($100ug_{Metal}$/ml in 10%FBS + DMEM) and 100ul alamarBlue assay. Cultures were incubated for 24 hr each, then medium was collected for spectrometry. Each condition had 4 wells.

[Further details of the crystal structure investigation(s) may be obtained from the JCPDS 00-019-0629 (Fe_3O_4) and JCPDS 04-015-9870 ($CoFe_2O_4$)]

Supplementary Material

Refer to Web version on PubMed Central for supplementary material.

Acknowledgements

This work was funded in part by DARPA ElectRx Program (HR0011-15-C-0155), the Bose Research Grant, and the NIH BRAIN Initiative (1R01MH111872). This work made use of the MIT MRSEC Shared Experimental Facilities under award number DMR-14-19807 from the National Science Foundation. J.M. and S.P. are recipients of the Samsung Scholarship. S.R. is a recipient of the Simons Fellowship and funded by NIH (1K99MH120279-01). D.R. is a recipient of the MIT-Technion Fellowship.

References

[1]. Yoo D, Jeong H, Noh S-H, Lee J-H, Cheon J, Angew. Chemie Int. Ed 2013, 52, 13047.

[2]. Huang H, Delikanli S, Zeng H, Ferkey DM, Pralle A, Nat Nano 2010, 5, 602.

[3]. Chen R, Romero G, Christiansen MG, Mohr A, Anikeeva P, Science 2015, 347, 1477. [PubMed: 25765068]

[4]. Christiansen MG, Senko AW, Chen R, Romero G, Anikeeva P, Appl. Phys. Lett 2014, 104, 213103.

[5]. Carrey J, Mehdaoui B, Respaud M, J. Appl. Phys 2011, 109.

[6]. Hergt R, Dutz S, J. Magn. Magn. Mater 2007, 311, 187.

[7]. Lee J-H, Jang J, Choi J, Moon SH, Noh S, Kim J, Kim J-G, Kim I-S, Park KI, Cheon J, Nat Nano 2011, 6, 418.

[8]. O'Handley RC, Modern magnetic materials: principles and applications; Wiley, 2000.

[9]. Song Q, Zhang ZJ, J. Phys. Chem. B 2006, 110, 11205. [PubMed: 16771385]

[10]. Slonczewski JC, Phys. Rev 1958, 110, 1341.

[11]. Tachiki M, Prog. Theor. Phys 1960, 23, 1055.

[12]. Cao E, Cordero-Morales JF, Liu B, Qin F, Julius D, Neuron 2013, 77, 667. [PubMed: 23439120]

[13]. Akerboom J, Chen T-W, Wardill TJ, Tian L, Marvin JS, Mutlu S, Calderón NC, Esposti F, Borghuis BG, Sun XR, Gordus A, Orger MB, Portugues R, Engert F, Macklin JJ, Filosa A, Aggarwal A, Kerr RA, Takagi R, Kracun S, Shigetomi E, Khakh BS, Baier H, Lagnado L, Wang SS-H, Bargmann CI, Kimmel BE, Jayaraman V, Svoboda K, Kim DS, Schreiter ER, Looger LL, J. Neurosci 2012, 32, 13819 LP. [PubMed: 23035093]

[14]. Chen R, Christiansen MG, Anikeeva P, ACS Nano 2013, 7, 8990. [PubMed: 24016039]

[15]. Yu WW, Chang E, Falkner JC, Zhang J, Al-Somali AM, Sayes CM, Johns J, Drezek R, Colvin VL, J. Am. Chem. Soc 2007, 129, 2871. [PubMed: 17309256]

[16]. Garaio E, Collantes JM, Plazaola F, Garcia JA, Castellanos-Rubio I, Meas. Sci. Technol 2014, 25, 115702.

[17]. Connord V, Mehdaoui B, Tan RP, Carrey J, Respaud M, Rev. Sci. Instrum 2014, 85.

[18]. Garaio E, Collantes JM, Garcia JA, Plazaola F, Mornet S, Couillaud F, Sandre O, J. Magn. Magn. Mater 2014, 368, 432.

[19]. Guibert C, Fresnais J, Peyre V, Dupuis V, J. Magn. Magn. Mater 2017, 421, 384.

[20]. Lenox P, Plummer LK, Paul P, Hutchison JE, Jander A, Dhagat P, IEEE Magn. Lett 2018, 9, 1.

[21]. Christiansen MG, Howe CM, Bono DC, Perreault DJ, Anikeeva P, Rev. Sci. Instrum 2017, 88.

[22]. Kobayashi H, Ueda K, Tomitaka A, Yamada T, Takemura Y, IEEE Trans. Magn 2011, 47, 4151.

[23]. Riedinger A, Guardia P, Curcio A, Garcia MA, Cingolani R, Manna L, Pellegrino T, Nano Lett. 2013, 13, 2399. [PubMed: 23659603]

[24]. Saint-Cricq P, Deshayes S, Zink JI, Kasko AM, Nanoscale 2015, 7, 13168. [PubMed: 26181577]

[25]. Varnavides G, Jermyn AS, Anikeeva P, Narang P, Phys. Rev. B 2019, 100, 115402.

[26]. Davis HC, Kang S, Lee J-H, Shin T-H, Putterman H, Cheon J, Shapiro MG, Biophys. J 2020, 118, 1502. [PubMed: 32061270]

[27]. Rosenfeld D, Senko AW, Moon J, Yick I, Varnavides G, Gregureć D, Koehler F, Chiang P-H, Christiansen MG, Maeng LY, Widge AS, Anikeeva P, Sci. Adv 2020, 6, eaaz3734. [PubMed: 32300655]

[28]. Munshi R, Qadri SM, Zhang Q, Castellanos Rubio I, Del Pino P, Pralle A, Elife 2017, 6.

[29]. Muir ER, Shen Q, Duong TQ, Magn. Reson. Med 2008, 60, 744. [PubMed: 18727091]

[30]. Caterina MJ, Schumacher MA, Tominaga M, Rosen TA, Levine JD, Julius D, Nature 1997, 389, 816. [PubMed: 9349813]

[31]. Romero G, Christiansen MG, Stocche Barbosa L, Garcia F, Anikeeva P, Adv. Funct. Mater 2016, 26, 6471.

[32]. Schuerle S, Dudani JS, Christiansen MG, Anikeeva P, Bhatia SN, Nano Lett. 2016, 16, 6303. [PubMed: 27622711]

[33]. Curcio A, Van de Walle A, Serrano A, Preveral S, Péchoux C, Pignol D, Menguy N, Lefevre CT, Espinosa A, Wilhelm C, ACS Nano 2020, 14, 1406. [PubMed: 31880428]

[34]. Liu JF, Neel N, Dang P, Lamb M, McKenna J, Rodgers L, Litt B, Cheng Z, Tsourkas A, Issadore D, Small 2018, 14, 1802563.

[35]. Chen R, Christiansen MG, Sourakov A, Mohr A, Matsumoto Y, Okada S, Jasanoff A, Anikeeva P, Nano Lett. 2016, 16, 1345. [PubMed: 26756463]

[36]. Yu WW, Chang E, Falkner JC, Zhang J, a Al-Somali M, Sayes CM, Johns J, Drezek R, Colvin VL, J. Am. Chem. Soc 2007, 129, 2871. [PubMed: 17309256]

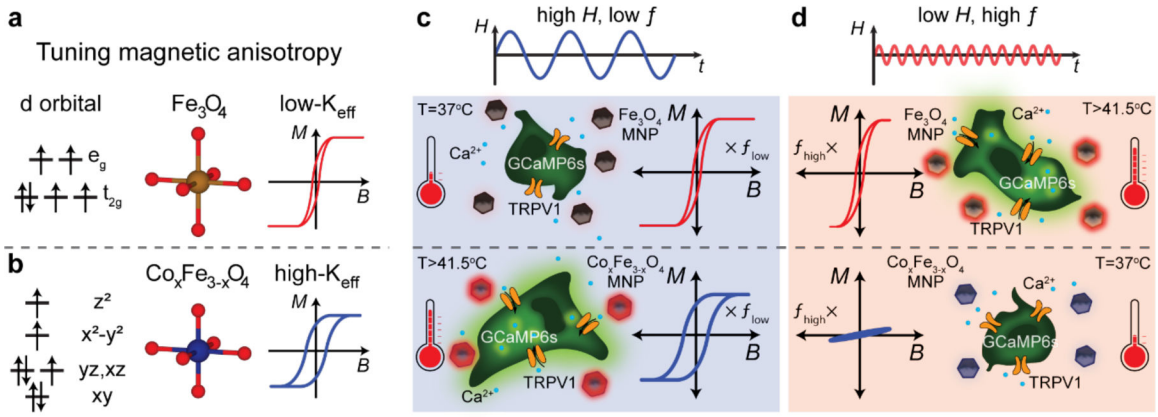

Figure 1.

Design of multiplexed control of cell signaling using selective magnetothermal stimulation. (a) and (b) Doping of cobalt into Fe_3O_4 results in higher magnetic anisotropy, making cobalt ferrite MNPs magnetically harder compared to Fe_3O_4. (c) and (d) Schematic representation of multiplexed magnetothermal control of cell signaling using two different MNP ensembles that respond selectively to paired AMF conditions. (c) A high-amplitude, low-frequency AMF is sufficient to access major hysteresis loops for both MNPs, with the major hysteresis loops of $Co_xFe_{3-x}O_4$ MNPs inherently larger, causing them to heat preferentially. (d) An AMF with low amplitude and high frequency results in major hysteresis loops only for less coercive MNPs (Fe_3O_4), and minor loops for $Co_xFe_{3-x}O_4$. The MNPs only dissipate heat effectively when they are exposed to their respectively paired AMF conditions, triggering the opening of the heat sensitive TRPV1 ion channels exogenously expressed in the HEK cells. Calcium ions flow into the cells through the activated TRPV1 channels and bind to GCaMP6s indicators, producing an increase in green fluorescence.

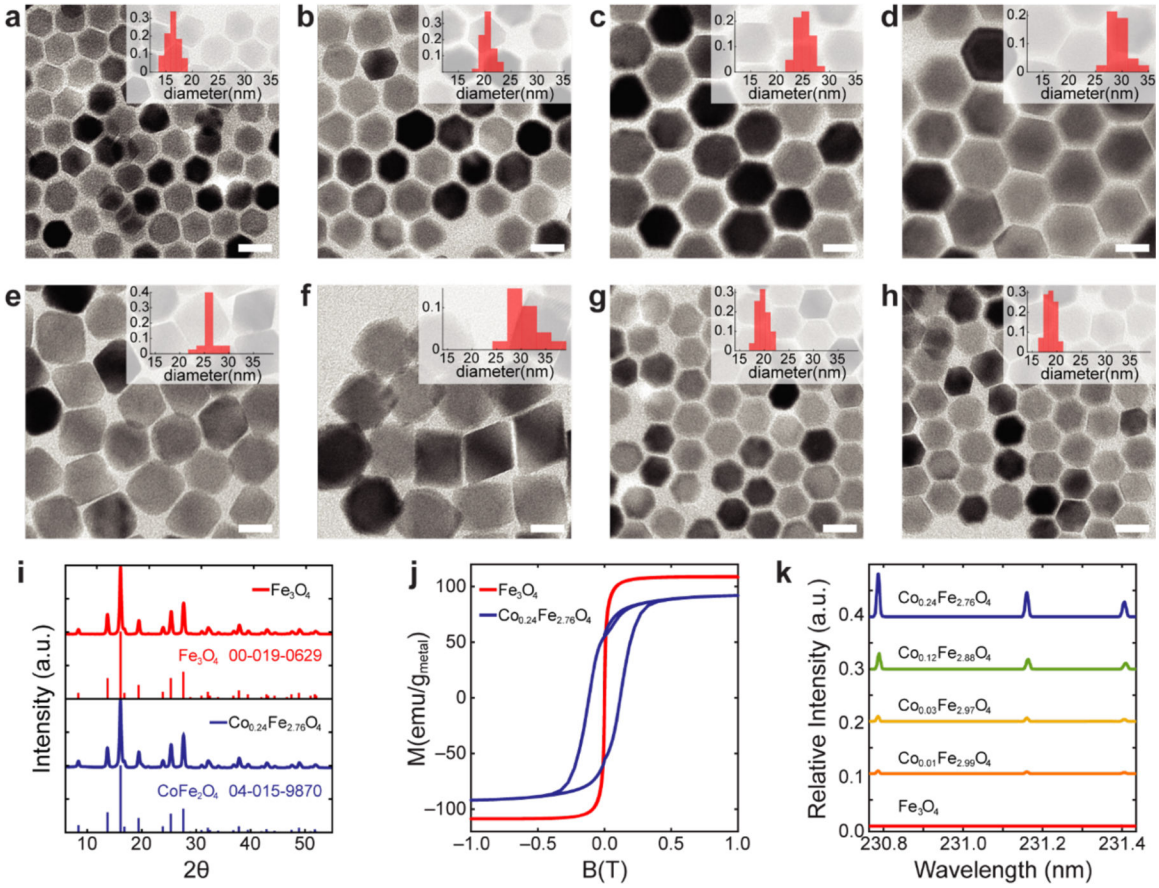

Figure 2.

Characterization of magnetic nanoparticles. (a-h), TEM of Fe_3O_4 (a-d) and $Co_xFe_{3-x}O_4$ (e-h) magnetic nanoparticles and their size distributions from TEM (inset histograms). (i) Powder XRD of Fe_3O_4 and $Co_xFe_{3-x}O_4$ nanoparticles indicates single-crystal structure (inverse spinel). (j) Magnetization data were collected with a SQUID magnetometer to confirm the difference between hard and soft MNPs. To exclude physical rotation of suspended magnetic particles in water, the measurement was performed at 260K. (k) Incorporated cobalt concentration in each ensemble was analyzed by ICP-AES. Each line shows relative cobalt intensity to iron intensity at 234.830nm.

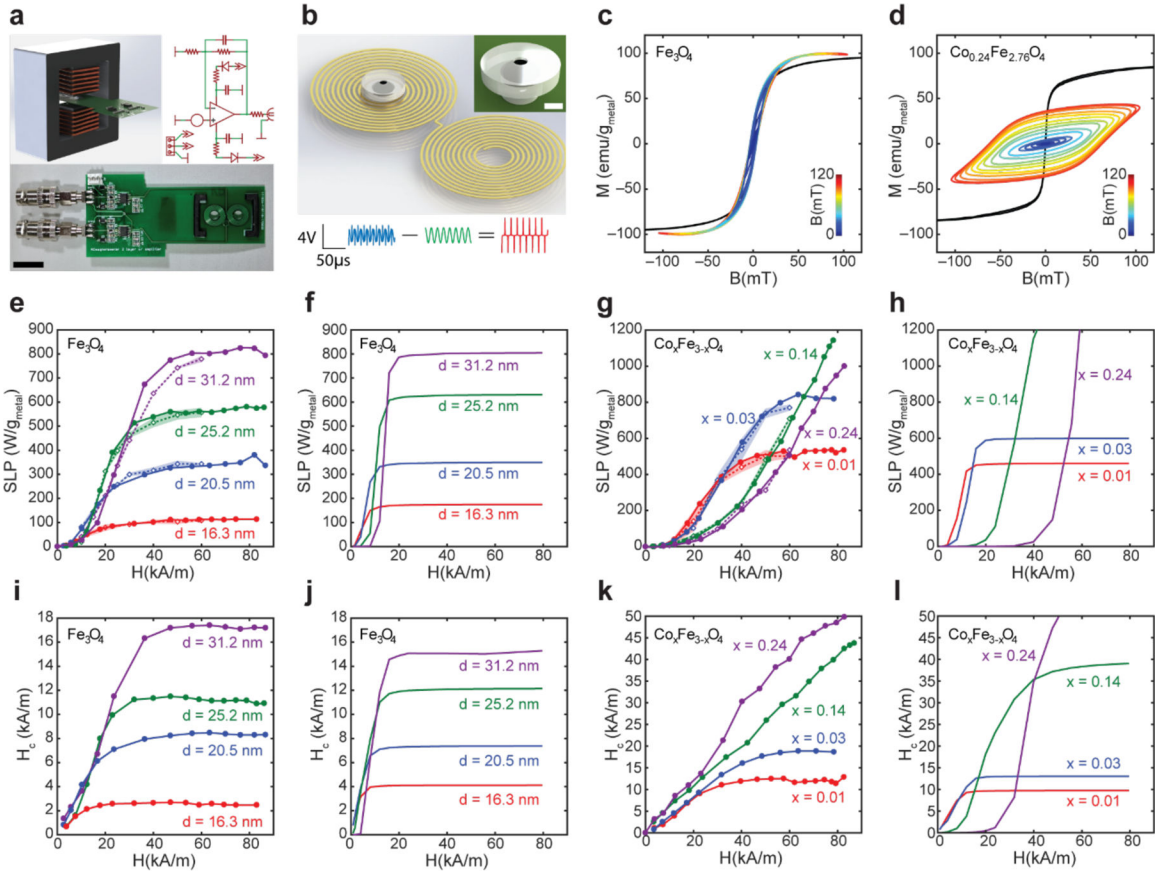

Figure 3.

Measurement of dynamic magnetization of MNP ensembles using custom high amplitude AC-magnetometer. (a) Design, photograph, and circuit diagram of the custom AC-magnetometer (ACM) used to capture dynamic magnetization under AMF. (Scale bar = 1 cm). (b) 2D coil design to detect dynamic magnetization. The spiral design of the sense coil results in a voltage induced by the changing magnetization of the sample. The compensation coil wound in the opposite direction cancels the majority of the voltage induced by the driving AMF. Ferrofluid is loaded into the 3D printed hollow spherical chamber of the sample holder. (Scale bar 1 = mm) (Blue – raw sample signal, Green – water control sample signal, Red – net sample signal). (Scale bars: voltage = 4V, time = 50 μs). (c, d) Dynamic hysteresis loops for ferrofluids of 16.2 nm Fe_3O_4 (c) and 16.3 nm $Co_{0.24}Fe_{2.76}O_4$ (d) were collected at room temperature under AMFs with f = 75 kHz and amplitudes ranging 0–120 mT. (Black line represents VSM data, jet color lines correspond to ACM data). (e-h), Specific loss power (SLP) of MNP ensembles measured empirically via ACM (e, g – solid lines, closed circle markers, measured at 75 kHz and linearly scaled by frequency to 101.2 kHz) and calorimetry (e, g - dashed lines, open diamond markers, shadowed areas represent standard deviation, measured at 101.2 kHz), and calculated via dynamic hysteresis model (f, h). (i-l) Coercive fields H_c for MNP ensembles calculated from ACM measurements (i, k) and simulated via the dynamic hysteresis model (j, l).

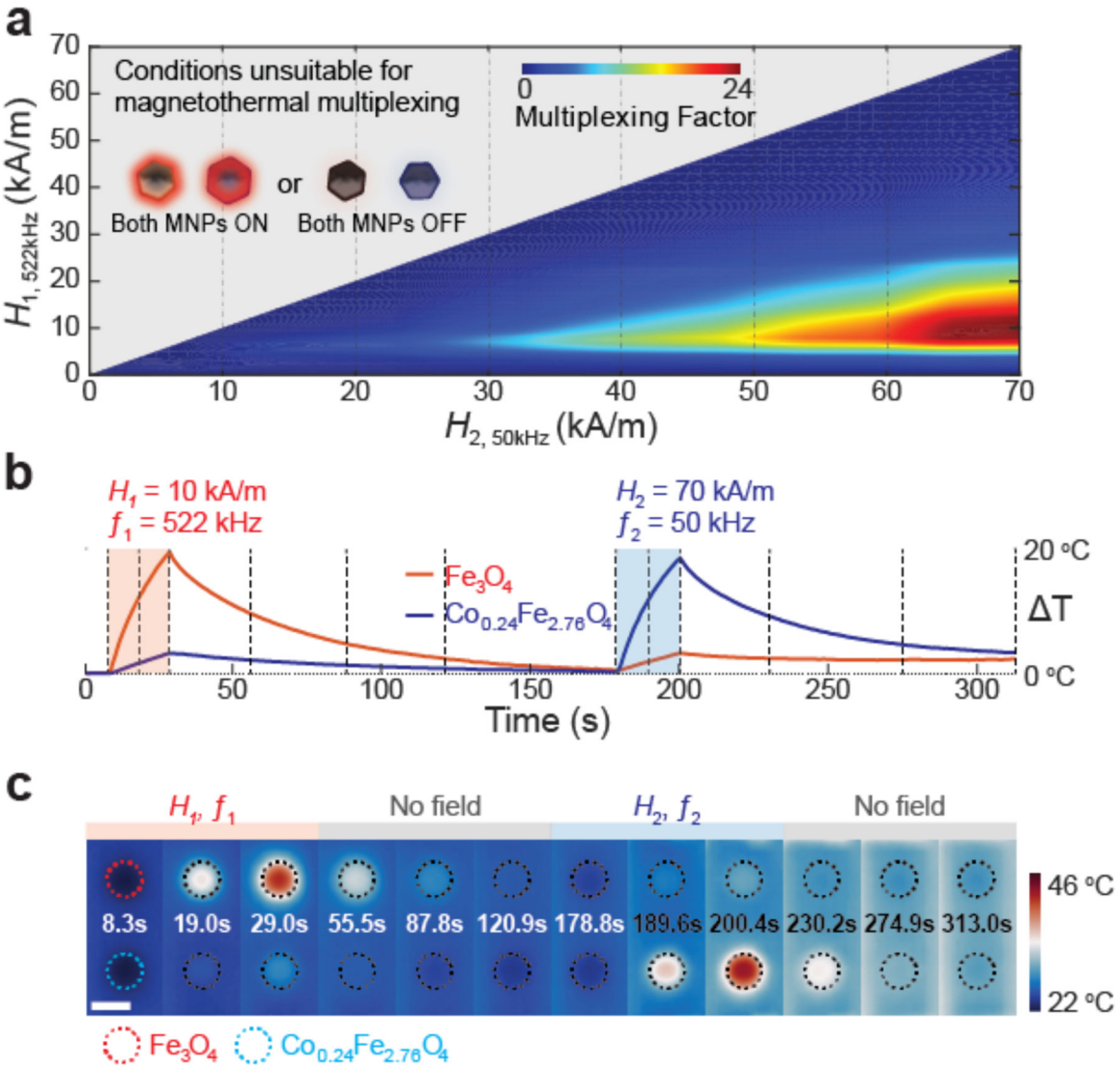

Figure 4.

Optimization of field conditions and thermographic verification for multiplexed thermal control (a) Multiplexing factor as a function of AMF amplitudes H_1 and H_2, for frequencies f_1=522 kHz and f_2=50 kHz. The grey area represents excluded conditions $H_1 > H_2$; a pair of AMFs in which both the amplitude and frequency of one condition is higher than the other is unsuitable for magnetothermal multiplexing. (b) Temperature profiles and (c) Thermographic images of two 10 μl MNP solution droplets (Fe_3O_4 16.3 nm - red and $Co_{0.24}Fe_{2.76}O_4$ 18.6nm - blue) exposed sequentially to two distinct AMFs for 20 s (70 kA/m, 50 kHz and 10 kA/m, 522 kHz), at each time frame. Dashed lines in temperature profiles (b) represent the times of the thermographic frames in (c). (Scale bar = 5 mm)

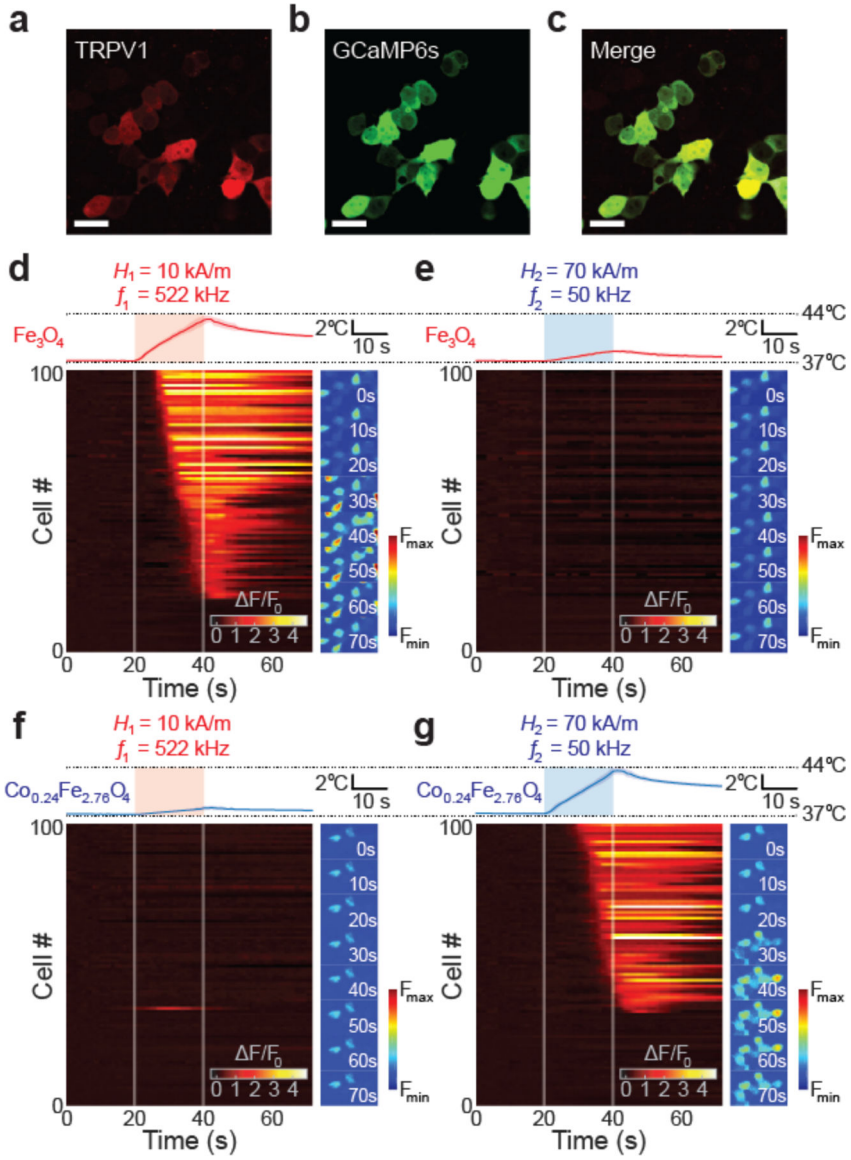

Figure 5.

Cellular responses selectively triggered by multiplexed magnetothermal control. (a-c) Confocal images of HEK293T cells co-transfected with both TRPV1-p2A-mCherry (a, c) cytoplasmic mCherry expression) and GCaMP6s (b, c). (Scale bar = 25 μm). (d-g) Cellular responses to multiplexed magnetothermal heating. Temperature profiles (upper plots) of the ferrofluids and the normalized GCaMP6s fluorescence $\Delta F/F_0$ (lower heat maps) of 100 randomly automatically chosen HEK239T cells plotted within the same time frame (0–70 s). Side panels indicate normalized GCaMP6s fluorescence images of the cells at different time-points during the experiments. (Scale bars = 40 μm). For each ferrofluid, the non-pairing AMF was applied at first. Afterward the same field of view (FOV) was imaged when cells were exposed to the pairing AMF. Each $\Delta F/F_0$ profile is from same FOV for each cover slip. AMFs were applied for 20 s (color boxes in temperature profiles and white lines in heat maps: from 20 s to 40 s). (d) Fe_3O_4 at 10 kA/m 522 kHz AMF. (e) Fe_3O_4 with 70

kA/m 50 kHz AMF. (f) $Co_{0.24}Fe_{2.76}O_4$ with 10 kA/m 522 kHz AMF. (g) $Co_{0.24}Fe_{2.76}O_4$ with 70 kA/m 50 kHz AMF.